Thermal noise of mechanical oscillators in steady states with a heat flux

Livia Conti,[1,*] Claudia Lazzaro,[1] Gagik Karapetyan,[1] Michele Bonaldi,[2,3] Matteo Pegoraro,[1] Ram-Krishna Thakur,[1] Paolo De Gregorio,[1] and Lamberto Rondoni[4,5]

[1]*Istituto Nazionale di Fisica Nucleare, Via Marzolo 8, I-35131 Padova, Italy*

[2]*Institute of Materials for Electronics and Magnetism, Nanoscience-Trento-FBK Division, 38123 Povo (Trento), Italy*

[3]*Istituto Nazionale di Fisica Nucleare, Trento Institute for Fundamental Physics and Applications, 38123 Povo (Trento), Italy*

[4]*Dipartimento di Scienze Matematiche and Graphene@PoliTO Lab, Politecnico di Torino Corso Duca degli Abruzzi 24, 10129 Torino, Italy*

[5]*Istituto Nazionale di Fisica Nucleare, Sezione di Torino, Via P. Giura 1, 10125 Torino, Italy*

(Received 19 February 2014; revised manuscript received 24 June 2014; published 17 September 2014)

We present an experimental investigation of the statistical properties of the position fluctuations of low-loss oscillators in nonequilibrium steady states. The oscillators are coupled to a heat bath, and a nonequilibrium steady state is produced by flowing a constant heat flux, setting a temperature difference across the oscillators. We investigated the distribution of the measurements of the square of the oscillator position and searched for signs of changes with respect to the equilibrium case. We found that, after normalization by the mean value, the second, third, and fourth standardized statistical moments are not modified by the underlying thermodynamic state. This differs from the behavior of the absolute, i.e., not normalized, second moment, which is strongly affected by temperature gradients and heat fluxes. We illustrate this with a numerical experiment in which we study via molecular dynamics the fluctuations of the length of a one-dimensional chain of identical particles interacting via anharmonic interparticle potentials, with the extremes thermostated at different temperatures: we use the variance of the length in correspondence to its first elastic mode of resonance to define an effective temperature which we observe to depart from the thermodynamic one in the nonequilibrium states. We investigate the effect of changing the interparticle potential and show that the qualitative behavior of the nonequilibrium excess is unchanged. Our numerical results are consistent with the chain length being Gaussian distributed in the nonequilibrium states. Our experimental investigation reveals that the position variance is the only, and crucially easily accessible, observable for distinguishing equilibrium from nonequilibrium steady states. The consequences of this fact for the design of interferometric gravitational wave detectors are discussed.

DOI: 10.1103/PhysRevE.90.032119 PACS number(s): 05.40.−a, 05.70.Ln, 04.80.Nn

I. INTRODUCTION

Knowledge of the probability density function (PDF) of stochastic observables is of key importance in experimental physics. Even the significance of the mean value and root-mean-square of an observable depends on some hypotheses about its statistical distribution. In the case of low signal-to-noise ratio experiments, such as in the search for gravitational waves [1], detailed knowledge of the spontaneous fluctuations is mandatory if one wants to distinguish the (small) signal from the noise. While equilibrium systems are well described by the Boltzmann-Gibbs distribution, an equivalent general framework valid for nonequilibrium systems is not available.

In the literature a wide set of experiments are dedicated to the study of the fluctuations in either transient or stationary states (see, for instance, Refs. [2–6]). From a theoretical viewpoint, the nonequilibrium states are characterized by the failure of the detailed balance. Experimentally, the nonequilibrium state is revealed either by a fictitious effective temperature, usually greater than the thermodynamic one, or by the non-Gaussianity of the observed distributions. In this context power-law distributions have attracted much attention because they are found in a very wide variety of contexts (see, for instance, the review [7]). However, the quantification of the absence of equilibrium is still a subject of research [8–10]. Therefore it is difficult to predict whether nonequilibrium phenomena will manifest in a given system and eventually to size them. Indeed, it is not even clear how to operationally identify a steady state, e.g., by setting an upper limit on the time derivative of thermodynamic quantities, such as temperature.

In Ref. [11] we reported the experimental investigation of the mean energy content of oscillators subject to constant heat fluxes. A schematics of the system under study is shown in Fig. 1 (see more details in Ref. [11]): an aluminium rod (length = 0.1 m) with square cross section is kept in the vertical position with the top end fixed and the bottom end loaded by a cuboid mass (mass $\sim$ 0.2 kg) which is free to vibrate. With a capacitive readout coupled to a low-noise amplifier we monitored the vibration fluctuations around the resonance of the first transverse and longitudinal acoustic modes, respectively at about $f_{m1} \sim 320$ Hz and $f_{m2} \sim 1420$ Hz: the elastic deformation corresponding to these modes is shown in panels b and c of Fig. 1. In the low-loss approximation, around their resonance these modes are realization of normal harmonic oscillators. The top end of the rod was connected to a thermal bath at temperature T_1 while the mass at the bottom was coupled to a heat source, which raises its temperature to T_2: thus, by flowing heat, we controlled the temperature difference $\Delta T = T_2 - T_1$ across the rod. Conduction is the dominant heat transfer mechanism. For the mentioned oscillators, in stationary states out of equilibrium, we observed an excess of the mean kinetic energy (averaged over periods of 0.5–1 h) with respect to the values expected from the thermodynamic

*Corresponding author: lconti@pd.infn.it

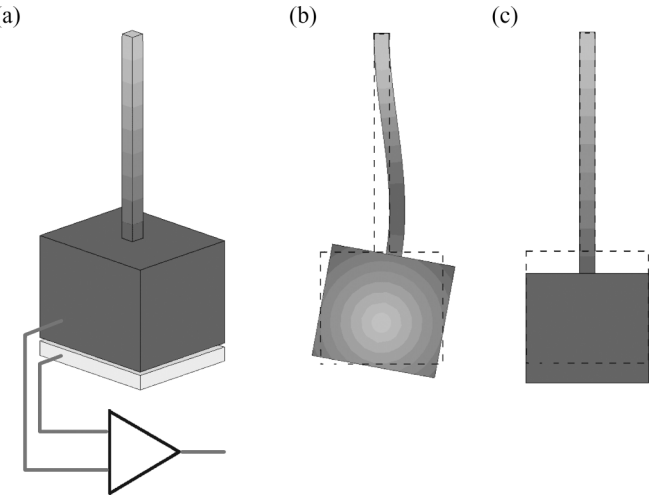

FIG. 1. (a) Schematic representation of the experimental setup. A metal rod with one end fixed and the other loaded by a mass free to vibrate is kept in the vertical position; the rod length is 0.1 m, and the mass weighs about 0.2 kg. A capacitive readout realized between the mass bottom surface and a facing fixed electrode monitors the mass vibrations: it is coupled to a custom low-noise amplifier, and then the signal is digitized and acquired. A thermal source facing the mass sets a thermal difference ΔT between the top and bottom end of the rod, respectively, at T_1 and T_2, $\Delta T = T_2 - T_1$. The thermal profile along the rod in the steady state is shown in gray shading (increasing temperature from light to dark). The deformation of the body is shown which corresponds to the transverse (b) and longitudinal (c) acoustic mode under study; the shape of the body at rest is shown with dashed lines for comparison. For parts (b) and (c) the gray scale shows the total deformation, which is larger at darker gray levels.

temperatures. In other words, in the presence of a heat flux along the piece, the mean kinetic energy noticeably exceeded even the maximum of the end temperatures. This shows that in the nonequilibrium state the energy equipartition does not hold: the low-frequency elastic modes show an energy content that depends on the nonequilibrium driving in addition to T and that exceeds the energy of the very high-frequency modes which originate the temperature T sensed by local thermometers.

We interpreted this excess in terms of correlations, caused by the heat flux, among the acoustic modes of the system. The excess is substantial even close to equilibrium, with relative temperature differences of the order of a few percent. Using a linear approximation for thermal conduction valid close to equilibrium, we derived an expression for the variance $\langle x^2\rangle_{\rm NEQ}$ of the position fluctuations of a single mode of vibration as a function of the nonequilibrium driving, i.e.:

$$\langle x^2\rangle_{\rm NEQ} = \frac{\eta}{\eta - \lambda(\phi)^2}\,\langle x^2\rangle_{\rm EQ}, \tag{1}$$

$$\lambda(\phi) = \frac{1}{2\phi}(1 - \sqrt{1 + 4\eta\phi^2}); \quad \eta = \frac{\mu}{M\omega_1^2(k_B T)^2}, \tag{2}$$

where $\langle x^2\rangle_{\rm EQ}$ is the variance in equilibrium at the average physical temperature T, ϕ is proportional to the nonequilibrium driving, being the fraction of heat transfer rate carried on average by the mode, η plays the role of a parameter which discriminates between the small and large driving regimes [see Eqs. (3) and (4) below], ω_1 is the mode resonant frequency, M is the mode mass, and μ is a mass parameter attributed to the other modes coupled with this one. It comprises a linear combination of all the other modes' masses contained in the heat flux term, and it reflects diagonalization of the Hamiltonian. μ is well approximated by a single-mode mass when the coupling with that one is much stronger than with all the others. In the limit of small or large driving, one finds

$$\langle x^2\rangle_{\rm NEQ} \simeq \langle x^2\rangle_{\rm EQ}\,(1 + \eta\,\phi^2); \quad |\phi| \ll 1/\sqrt{\eta}, \tag{3}$$

$$\langle x^2\rangle_{\rm NEQ} \simeq \langle x^2\rangle_{\rm EQ}\,\sqrt{\eta}\,|\phi|; \quad |\phi| \gg 1/\sqrt{\eta}. \tag{4}$$

In Ref. [11] we found that in the nonequilibrium states the effective temperature $T_{\rm eff} = M\omega_1^2\langle x^2\rangle_{\rm NEQ}$ becomes larger than the physical temperature and that the difference is of the same order of magnitude as T itself. The dependence on the square of ΔT similar to that in Ref. [12] suggests that the correlation among oscillators can be interpreted in terms of entropy production. For T fixed, letting $\phi = c\,\Delta T/T$ and $a = \eta\,c^2$, Eqs. (1) and (2) can be rewritten in dimensionless terms:

$$\zeta(s) = \frac{1}{2s}(1 - \sqrt{1 + 4as^2}), \tag{5}$$

$$R_{\rm NEQ/EQ} = \frac{\langle x^2\rangle_{\rm NEQ}}{\langle x^2\rangle_{\rm EQ}} = \frac{a}{a - \zeta(s)^2}; \quad s = \frac{\Delta T}{T}. \tag{6}$$

We note that the parameter a in Eq. (6) depends on the temperature of the system; indeed, our choice is to consider T as the average physical temperature, thus making a maximum error of order $O(\Delta T)$. Hence we expect the equation (6) to break down for large relative temperature differences.

We also performed a numerical experiment with a Fermi-Pasta-Ulam-like one-dimensional chain, with one end fixed and the other end free [13], each connected to a thermostat at temperature, respectively, T_1 and T_2, with $T_2 - T_1 \geqslant 0$ and $(T_1 + T_1)/2$ constant. The identical particles of the chain interacted with first- and second neighbors, via Lennard-Jones-type potentials of the kind [14]

$$V_{\rm LJ}(d) = V_{12,6}(d) = \epsilon\left[\left(\frac{d_0}{d}\right)^{12} - 2\left(\frac{d_0}{d}\right)^{6}\right], \tag{7}$$

where d is the distance between any two interacting particles, $d_0 = r_0$ for nearest neighbors, $d_0 = 2r_0$ for second neighbors, and r_0 is the particles' separation at $T = 0$. The Fourier analysis of the total length of the chain gave results very similar to those of the real experiment; moreover, the ratio between the total energy of the first mode of the chain in the nonequilibrium state with $T_2 - T_1 > 0$ around $(T_1 + T_1)/2$ and the total energy of the mode in equilibrium at the same $(T_1 + T_1)/2$ were well fitted by our theoretical model of Eq. (6) [11].

In this paper we investigate how the new energy distribution depends on the specific interparticle potential in our one-dimensional numerical model. Thus we perform the same numerical analysis described in Ref. [11] but with a potential different from that of Eq. (7). Moreover we investigate the statistics of the fluctuations of the position of low-loss oscillators in steady states due to constant heat fluxes. We stress that even for such a simple nonequilibrium system the probability distribution concerning microscopic

configurations is not known. To single out changes in the statistical distributions with respect to the equilibrium case, we study the second, third, and fourth moments of the statistical distribution of the square of the oscillator positions and compare the values obtained in the nonequilibrium states with those at equilibrium. We normalize the second moment (i.e., the variance) to the mean value, to focus on its statistical distribution, rather on its mean value. The position variance, used in Ref. [11] to characterize the oscillator effective energy, is proved here to be the only easily accessible parameter that needs consideration in high-sensitivity experiments, as the gravitational wave detectors, in order to account for the subtle dissipation effects taking place in such instruments. We conclude the paper with a prediction of the nonequilibrium effect in gravitational wave detectors.

II. NUMERICAL MODEL

The numerical model discussed in Ref. [11] gives results which agree both with the theoretical model and with the experimental finding for the longitudinal mode. To assess whether such agreement is accidental or the sign of a more general behavior, we consider here a second model which differs that of Ref. [11] for the interparticle potential different from V_L. In the present study we investigate the chain with the potential

$$V_{12,8}(d) = \epsilon\left[2\left(\frac{d_0}{d}\right)^{12} - 3\left(\frac{d_0}{d}\right)^{8}\right], \tag{8}$$

which is equal to Eq. (7) in the repulsive part and has the same energy depth ϵ. At the lowest temperatures one can approximate:

$$\begin{aligned} V_{\mathrm{LJ}}(d) &\simeq \tfrac{1}{2}k_{el}(d-d_0)^2 = 36\,\epsilon\,(d-d_0)^2, \\ V_{12,8}(d) &\simeq \tfrac{1}{2}k'_{el}(d-d_0)^2 = 48\,\epsilon\,(d-d_0)^2. \end{aligned} \tag{9}$$

Thus in the two cases the elastic constants differ by about 30%. The time evolution of the length of a chain of 128 identical particles interacting via potential $V_{12,8}$ is studied via molecular dynamics techniques; as in Ref. [11], one of the chain ends is fixed and thermostatted at T_1 while the other is left free and thermostatted at T_2, with $\Delta T = T_2 - T_1 \geqslant 0$ and $(T_1 + T_2)/2 = T_{\mathrm{avg}}$ constant. The Fourier analysis of the length chain allows us to estimate the mean energy of its first mode of resonance.

The ratio $R_{\mathrm{NEQ/EQ}}$ defined in Eq. (6) is plotted in Fig. 2; for a better comparison in the same figure we also show the results obtained in Ref. [11] with the potential V_{LJ}. The nonequilibrium driving has a dramatic impact on the mode energy, i.e., on the variance of the mode coordinate: with just a 10% thermal difference the variance increases by a factor of about two with the potential $V_{12,8}$. Each set of numerical data is fitted with the one-parameter curve of Eq. (6), and the results are also shown in Fig. 2. The change of the interparticle potential does not lead to qualitatively different results: quantitatively the change is also limited, and the agreement with our theoretical model of Eq. (6) remains good.

We conclude this section with a test of the hypothesis that the chain length $z(t)$ is Gaussian distributed even in the nonequilibrium states: we stress that this is not a test for the

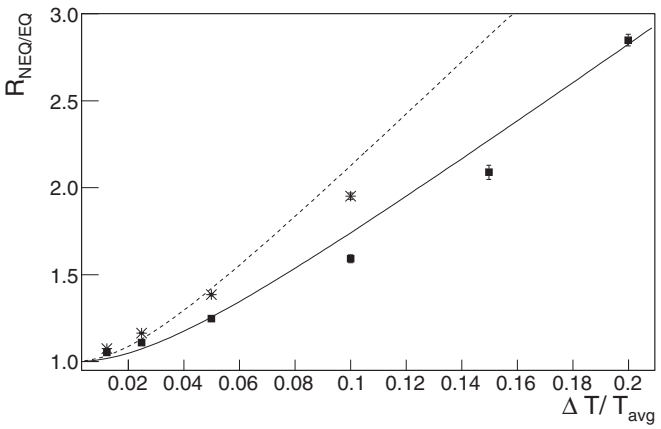

FIG. 2. Plot of the ratio $R_{\mathrm{NEQ/EQ}}$ as function of the relative temperature difference across the one-dimensional chain. The stars (respectively, squares) show the results obtained with the interparticle potential $V_{12,8}$ (respectively, V_{LJ}); the dashed (respectively, solid) line is the fit of the data with the theoretical model of Eq. (6). The fit results in $a = 240 \pm 3$ for $V_{12,8}$ and $a = 129 \pm 2$ for V_{LJ}.

distribution only of the first modes of the chain (as with the experiment; see Sec. IV) but in the whole frequency range, i.e., for every frequency ω. This is possible due to the fact that in the numerical simulations there are no external noise forces, except for the algorithmic baths; this differs from the real experiment, where the normal modes emerge from the electronic noise only near their resonances. With this in mind, we analyze the indeterminacy which accompanies the estimation of the power spectra, which is directly related to the probability distribution of the variable $z(t)$. Although we used FFT for the calculations, in the following the underlying theory is derived in the continuum limit and for frequencies $\omega \neq 0$ (a more complete derivation can be found in Ref. [15]).

Consider the following (stochastic) variable:

$$\mathcal{X}(\omega) = z(0)\int_{-\infty}^{+\infty} e^{i\omega t} z(t)\,dt = z(0)\tilde{z}(\omega). \tag{10}$$

$\mathcal{X}$ can be thought of as the spectral decomposition in a single simulation run or in a single time buffer. The mean of $\mathcal{X}$ is obtained by averaging over many runs or buffers, and it is by definition the power spectral density $S(\omega)$ of the position

$$S(\omega) = \langle \mathcal{X}(\omega) \rangle. \tag{11}$$

Here we are interested in the variance of $\mathcal{X}$, which allows us to estimate the sample standard deviation in a series of runs or buffers.

With the hypothesis that $z(t)$ is a fully Gaussian process with zero mean, it follows that four-point averages can be decomposed into the sum of products of two-point averages, in the following way:

$$\begin{aligned} &\langle z(t_1)z(t_2)z(t_3)z(t_4)\rangle \\ &\quad = \langle z(t_1)z(t_2)\rangle\langle z(t_3)z(t_4)\rangle + \langle z(t_1)z(t_3)\rangle\langle z(t_2)z(t_4)\rangle \\ &\qquad + \langle z(t_1)z(t_4)\rangle\langle z(t_2)z(t_3)\rangle. \end{aligned} \tag{12}$$

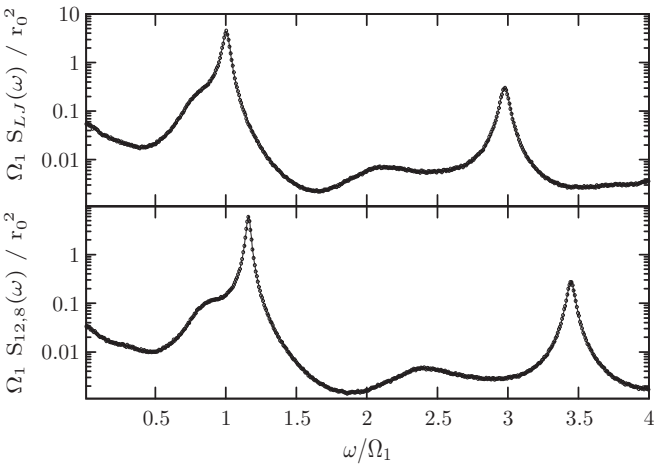

FIG. 3. Simulations with relative gradient of 10%. Comparison of $S(\omega) = \langle \mathcal{X}(\omega) \rangle$ (solid lines) and $\sigma_{\mathcal{X}}(\omega) = \sqrt{\langle \mathcal{X}^2(\omega) \rangle - S^2(\omega)}$ ($\circ$ points), for the interparticle potentials V_{LJ} (top panel) and $V_{12,8}$ (bottom panel): for both potentials, the difference can hardly be appreciated, being less than 5%. Ω_1 stands for the resonance frequency ω_1 of the first mode in the specific case of the LJ potential, and it serves as normalization for comparison.

In order to get the variance of $\mathcal{X}$, we need first to evaluate the mean of

$$\mathcal{X}^2(\omega) = z^2(0) \int_{-\infty}^{+\infty} \int_{-\infty}^{+\infty} e^{i\omega t} z(t) e^{i\omega t'} z(t')\, dt\, dt', \qquad (13)$$

which, due to the Gaussian decomposition, leads to

$$\langle \mathcal{X}^2(\omega) \rangle = 2S^2(\omega) + \langle z^2(0) \rangle \int_{-\infty}^{+\infty} \int_{-\infty}^{+\infty} e^{i\omega(t+t')} \langle z(t) z(t') \rangle\, dt\, dt'. \qquad (14)$$

The second term on the r.h.s. of this equation is null in stationary states, by virtue of the equalities $\langle z(t) z(t') \rangle = \langle z(t - t') z(0) \rangle$ and $\langle z(0) z(\tau) \rangle = \langle z(0) z(-\tau) \rangle$, which imply for $\omega \neq 0$

$$\begin{aligned} &\int_{-\infty}^{+\infty} \int_{-\infty}^{+\infty} e^{i\omega(t+t')} \langle z(t) z(t') \rangle\, dt\, dt' \\ &= \frac{1}{2} \int_{-\infty}^{+\infty} dt e^{2i\omega t} \left[\int_{-\infty}^{+\infty} e^{i\omega\tau} \langle z(0) z(\tau) \rangle\, d\tau \right. \\ &\quad \left. - \int_{-\infty}^{+\infty} e^{-i\omega\tau} \langle z(0) z(\tau) \rangle\, d\tau \right] \\ &= -\frac{1}{2} \int_{-\infty}^{+\infty} dt e^{2i\omega t} \left[\int_{-\infty}^{+\infty} e^{i\omega\tau} \langle z(0) z(\tau) \rangle\, d\tau \right. \\ &\quad \left. - \int_{-\infty}^{+\infty} e^{-i\omega\tau} \langle z(0) z(\tau) \rangle\, d\tau \right] = 0. \end{aligned} \qquad (15)$$

It follows for the variance of $\mathcal{X}(\omega)$

$$\sigma_{\mathcal{X}}^2(\omega) = \langle \mathcal{X}^2(\omega) \rangle - \langle \mathcal{X}(\omega) \rangle^2 = S^2(\omega). \qquad (16)$$

Thus, if $z(t)$ is a Gaussian process, the sample standard deviation of the power spectrum equals the power spectrum itself. We use this equality as a test of Gaussianity of the chain length in the nonequilibrium states. In Fig. 3 we compare the two quantities in the case of both the interparticle potentials: the curve $\sigma_{\mathcal{X}}(\omega) = \sqrt{\langle \mathcal{X}^2(\omega) \rangle - S^2(\omega)}$ is indistinguishable from the power spectrum of the simulations, the relative difference being always smaller than 5%. Thus this property shows that in the nonequilibrium states our numerical results are consistent with the Gaussian hypothesis.

III. EXPERIMENTAL DATA ANALYSIS PROCEDURE

The signal of the capacitive readout that senses the position fluctuations of the metal rod (see Fig. 1) is dominated at low frequency by the mechanical noise of the floor: a suspension system which supports the experimental apparatus is effective in reducing the noise level to a negligible level above about 200 Hz. To isolate the contribution of the two modes (in the following referred to as mode 1, $m1$, for the transverse mode and mode 2, $m2$, for the longitudinal mode), the time series s_i of the acquired signal, which is the output of the amplifier following the capacitive readout, was filtered via a lock-in analysis: for each mode, two time series x_{mj}, y_{mj} ($j = 1,2$) were formed by multiplying the input signal with in-phase and in-quadrature component of a reference signal:

$$\begin{aligned} x_{mj}^* &= s_i \cos(2\pi f_{\mathrm{lck},j} t_i), \\ y_{mj}^* &= s_i \sin(2\pi f_{\mathrm{lck},j} t_i), \end{aligned} \qquad (17)$$

where $f_{\mathrm{lck},j}$ is the lock-in frequency and is chosen to match f_{mj}; $t_{i+1} - t_i$ is the inverse of the sampling frequency $f_s = 8$ kHz of the data acquisition. The resulting time series were then filtered in the frequency domain, multiplying the FFT of signal and filter: this is a low-pass Kaiser filter. The standard overlap-save method was used to divide the data in overlapping buffers and to perform the convolution. The resulting signals were then decimated to decorrelate for the filter frequency width: the decimation factor was three times the lock-in filter time width, i.e., 10 s for the transverse mode ($m1$) and 0.6 s for the longitudinal mode ($m2$). We refer to the filtered, decimated time series as x_{mj} and y_{mj} corresponding, respectively, to x_{mj}^* and y_{mj}^* of Eq. (17).

To guarantee that the lock-in is centered at the mode resonance, we updated the lock-in frequency $f_{\mathrm{lck},j}$ every 32 and 55 min for $m1$ and $m2$, respectively: we made it coincident with the value of the resonant frequency estimated by the Lorentzian fit of the time-averaged power spectral density. The procedure leading to the resonant frequency estimates is described in Ref. [11].

The signals x_{mj} and y_{mj} describe the oscillator position with respect to the reference sinusoidal curve. We combined them in quadrature to get a quantity proportional to the energy of the oscillator:

$$r_{mj}^2 = x_{mj}^2 + y_{mj}^2 \qquad (18)$$

with $j = 1,2$. The phase with respect to the reference signal is obtained by the arctangent function $\phi_{mj} = \mathrm{atan2}\left(y_{mj}, x_{mj}\right)$, which is expected to be uniformly distributed in the range

$(-\pi, +\pi]$. If the signals of Eq. (17) are independent and Gaussian distributed, as expected for an equilibrium oscillator, then r^2_{mj} follows a chi-square distribution of order 2, i.e., the exponential law of the canonical ensemble. To conform with Ref. [11], rather than studying the statistical distribution of x_{mj} and y_{mj}, we chose to study the distribution of r^2_{mj} and ϕ_{mj}.

The data of each decimated time series produced by the lock-in filters were grouped in time buffers lasting Δt_{mj}: for each buffer we computed the first moments of the statistical distribution of the data. The durations of the long buffers of the decimated data were chosen as a compromise between the need to have many buffers, i.e., many independent measurements of the statistics moments, and the need to populate sufficiently the buffer so that the measurements of the moments per buffer were significant. The time buffer lengths were $\Delta t_{m1} \sim 5$ h and $\Delta t_{m2} \sim 1$ h. Further, we discarded all decimated data buffers that did not satisfy the steady state condition of the maximum normalized total time derivative of the temperatures at the rod ends, which we set to 10^{-7} s^{-1}: this procedure was detailed in Ref. [14] and corresponds roughly to impose an upper limit of 20 μK/s on the instantaneous time derivative of the temperature.

IV. RESULTS ON FLUCTUATION STATISTICS

Figure 4 shows the histograms of the normalized variance, skewness, and excess kurtosis for the equilibrium states of the r^2_{mj} signals, for the $m1$ and $m2$ oscillators: in agreement with the expectations for an exponential distribution, on average the variance normalized to the square of the mean value, the skewness, and the excess kurtosis are compatible

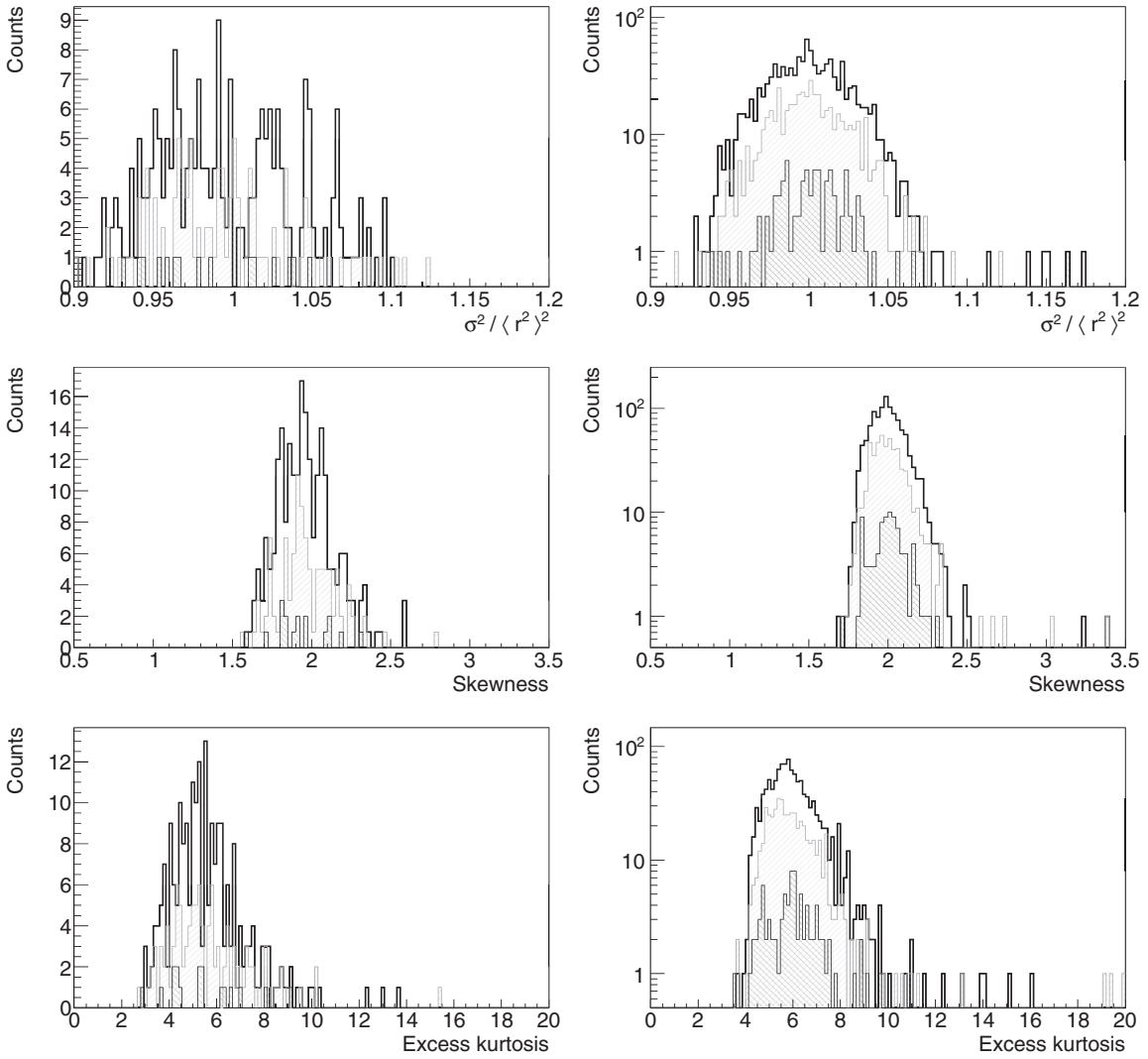

FIG. 4. Histograms of the measurements of the distribution's variance normalized to the (square of the) mean value (top row), skewness (middle row), and excess kurtosis (bottom row) in different thermodynamic states. Left column shows the results for r^2_{m1}: right column shows the results for r^2_{m2}. The solid line, white histograms, show the equilibrium measurements with $\Delta T = 0$ K (respectively, 232 and 1138 measurements for r^2_{m1} and r^2_{m2}); the dashed line, filled histograms, show the nonequilibrium measurements with $\Delta T = 9.4$ K (respectively, 110 and 522 measurements for r^2_{m1} and r^2_{m2}); the cross-filled histograms show the nonequilibrium measurements with $\Delta T = 13.2$ K (respectively, 17 and 87 measurements for r^2_{m1} and r^2_{m2}). Data taken at different values of thermal difference ΔT are not shown as they amount to fewer samples.

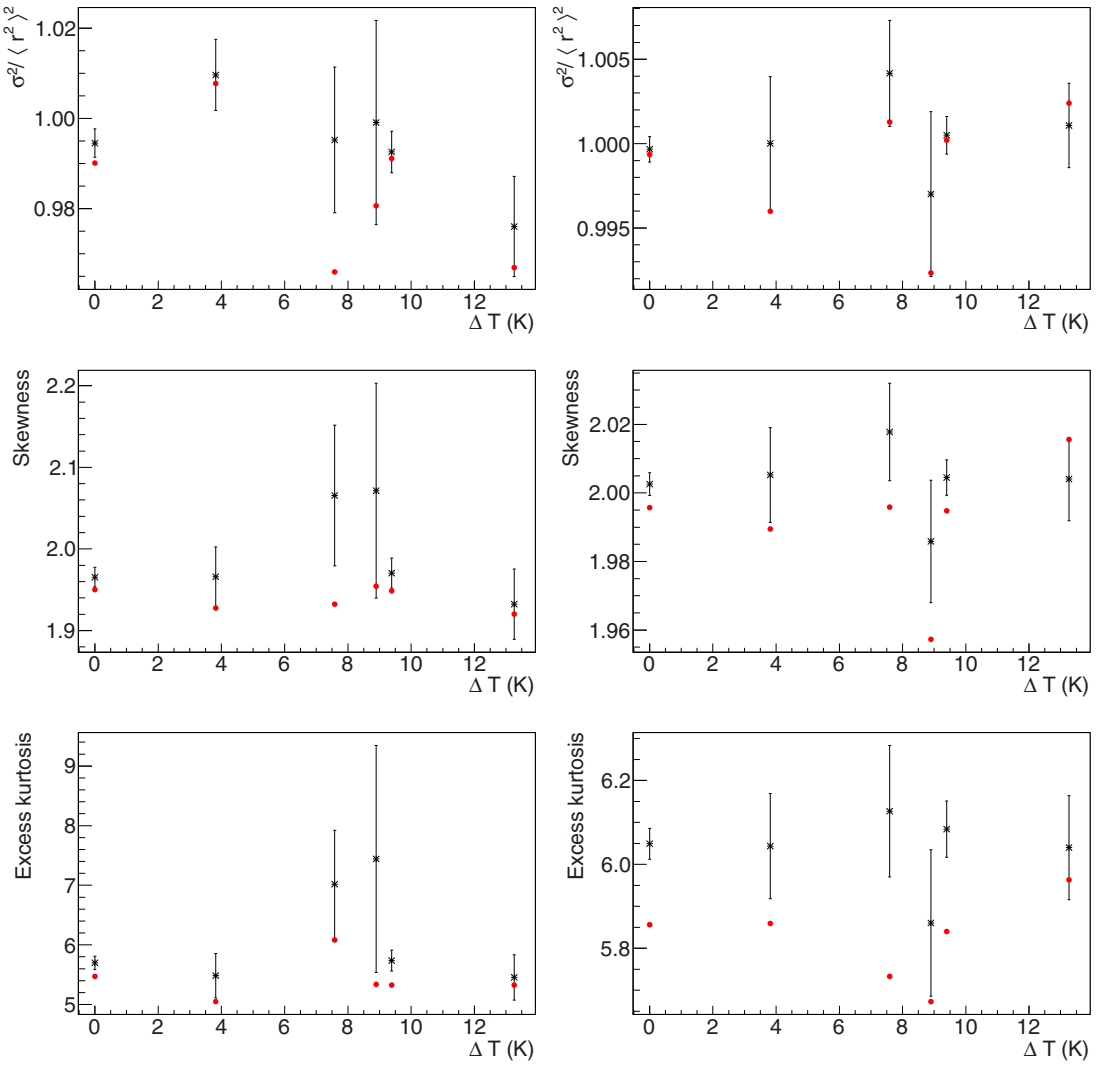

FIG. 5. (Color online) Plot of the normalized variance (top row), average skewness (middle row), and excess kurtosis (bottom row) as a function of the steady-state thermal difference ΔT. Left column shows the result for r^2_{m1}; right column shows the results for r^2_{m2}. The (black) crosses show the mean value of the measurements with their error bars; the (red) circles show the median of the measurements.

with the values 1, 2, and 6, respectively. The distribution of the kurtosis is slightly asymmetric, with a tail at high kurtosis values.

The good quality of these equilibrium states encouraged us to try to detect subtle changes in the PDF, which may arise when nonequilibrium sets in. We computed the normalized variance, skewness, and excess kurtosis for the data acquired in the nonequilibrium steady states: the histograms are shown in Fig. 4 for the $m1$ and $m2$ modes. The centers of the histograms seem not to have changed with respect to the equilibrium case. This is summarized in Fig. 5 where the average values of the normalized moments are plotted against the temperature difference between the two ends of the rod, a quantity proportional to the heat flux, i.e., to the nonequilibrium driving, in our near equilibrium conditions. To account for the asymmetry of the excess kurtosis histograms shown in Fig. 4, along with the mean value we also plot the median, which is less dependent on outliers: we note that the median is computed using all the data, i.e., without applying the above mentioned cutoff on the skewness.

Overall, apart from the reported significant dependence of the variance on the temperature difference [11], even at our maximum driving we see no other changes in the statistical distribution of the oscillators fluctuations, with respect to the equilibrium case.

The histograms of Fig. 4 do not show 3 and 33 momentum measurements for the r^2_{m1} and r^2_{m2}, respectively (corresponding to about 1%–2% of the measurements), which exceed the plot range (excess kurtosis >20) but which were collected in time periods passing the above mentioned steady-state criterion. In some cases these measurements occurred when also the front-end amplifier was disturbed, often by human intervention. However, not all occurrences can be related to some external recorded disturbances in the experimental apparatus: thus they cannot be vetoed with a criterion independent of the same signals r^2_{mj}. On the other hand, in this work we do not focus on the extreme value distribution but rather on the mean distribution of the position fluctuations of the oscillators. Thus when computing the mean momentum shown in Fig. 5 we decided to discard such time periods, vetoing those buffers in

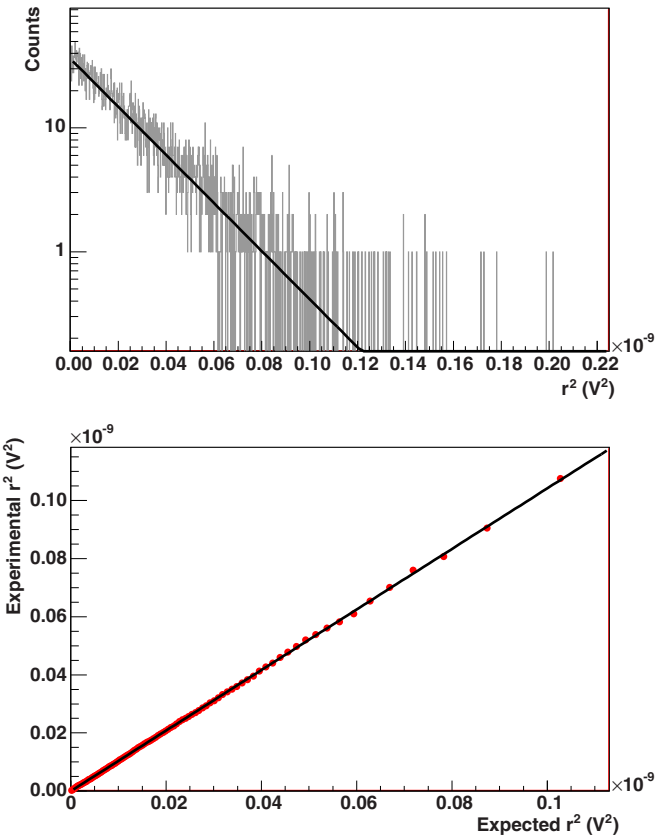

FIG. 6. (Color online) Top: Histogram of the decimated r^2_{m2} measurements collected during a buffer lasting Δt_{m2} at $\Delta T = 13.2$ K. The line is the exponential fit of the histogram. Bottom: QQ plot of the r^2_{m2} measurements shown on the left against the exponential distribution expected from their exponential fit. The last point corresponds to 99% probability. The line shows the linear fit of the QQ plot: the intercept is $(-4.0 \pm 3.5) \times 10^{-14}$, and the angular coefficient is 1.042 ± 0.001.

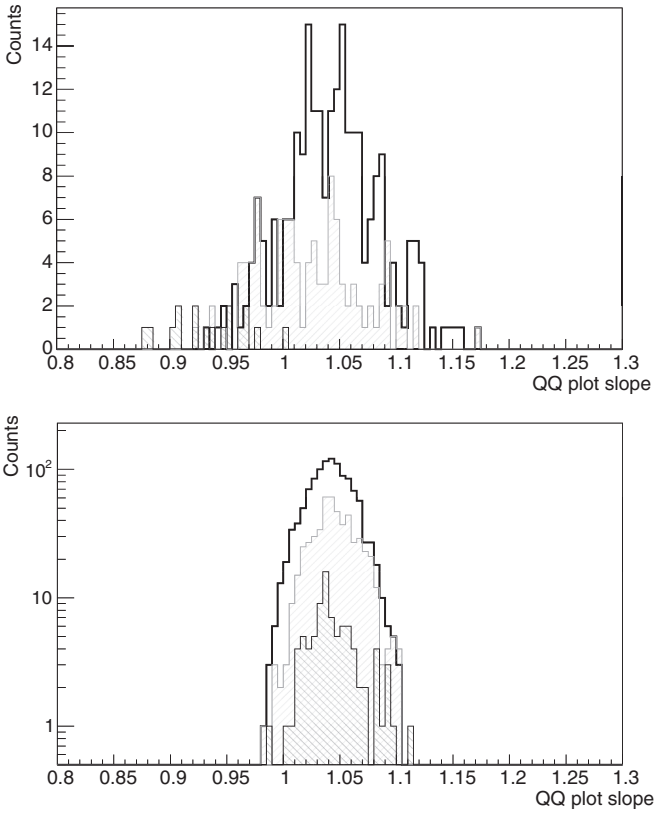

FIG. 7. Histograms of the angular coefficients of the lines fitting the QQ plots of the r^2_{mj} measurements against the exponential distribution: the exponents of the latter come from the fits of the experimental distributions. The legend for the histograms is the same as in Fig. 4, to distinguish measurements taken in different thermodynamic states. Top and bottom plots refer, respectively, to oscillator $m1$ and $m2$.

which excess kurtosis was larger than 30. We also note that the same criterion was applied to both oscillators, and to both equilibrium and nonequilibrium data: however, there seems to be no correlation between the thermodynamic state and the occurrence of these extreme outliers. Finally, the cutoff is so loose that any continuous modification of the moments with increasing nonequilibrium driving would be observed in any case. To also account for the small asymmetry of the distribution of the excess kurtosis shown in Fig. 4, we computed also the median of all the histogram data, removing the cutoff on the excess kurtosis. The median is less sensitive to extreme outliers than the mean. The result, however, is similar: no change is observed in the statistical distribution when the state departs from equilibrium, except for the variance of the oscillator fluctuations.

As a further test for measuring changes in the statistical distributions, we constructed quantile-quantile (QQ) plots: for each buffer of the decimated data we compared the quantiles of the experimental data with those expected for an equal number of samples following exactly the exponential law with the parameters coming from the exponential fit of the data. In all QQ plots we arranged the data in 1% probability bins. As an example, we show in the top part of Fig. 6 the histogram of the decimated r^2_{m2} measurements corresponding to a buffer of length Δt_{m2} taken with $\Delta T = 13.2$ K; the histogram is fitted by an exponential law, and the fit parameters are used to construct the horizontal axis in the corresponding QQ plot, shown in the bottom part of Fig. 6. All QQ plots are fitted with a line, and the resulting angular coefficients are collected in the histograms of Fig. 7 for the equilibrium and the nonequilibrium states. The mean angular coefficient is about 5% higher than expected, likely due to the limited statistics in the histograms. However, we observed no changes in the mean angular coefficient with the thermodynamic state, confirming the above conclusions.

As a control we also studied the statistical properties of the phases ϕ_{mj} with respect to the reference signal ($j = 1,2$): in equilibrium the oscillators are expected to have a random phase with respect to such reference. Thus in equilibrium the phase measurements are expected to follow a uniform distribution from $-\pi$ to π, with variance equal to 3.29 rad^2, null skewness, and excess kurtosis equal to -1.2. The mean value, variance, skewness, and excess kurtosis of the decimated ϕ_{mj}, $j = 1,2$, are shown in Fig. 8 for both equilibrium and nonequilibrium steady states. For clarity, in the figure no distinction is made for the different nonequilibrium levels ΔT. The expectations are well satisfied, in both the equilibrium and nonequilibrium states.

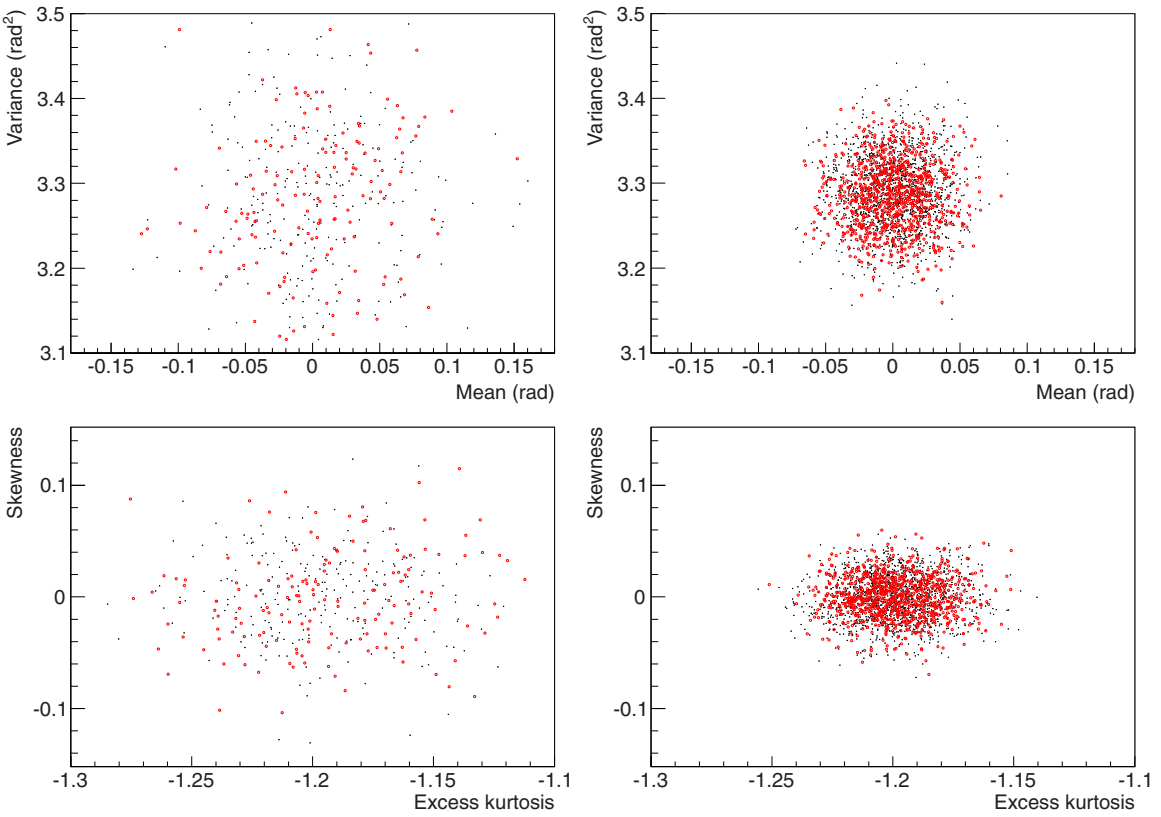

FIG. 8. (Color online) Plot of the variance vs mean value (top row) and of the skewness vs excess kurtosis (bottom row) for the phases ϕ_{m1} (left column) and ϕ_{m2} (right column). In the plots the (black) dots show the measurements in equilibrium, and the (red) open circles show the measurements in all the nonequilibrium steady states.

In the realm of nonequilibrium physics, one popular way to quantify variations of the PDF with respect to the equilibrium case is based on the value of the parameter q that defines the q analog of the equilibrium distributions, known as the q distributions (also known as Tsallis distributions [16]). In this context a q value of 1 implies no changes with respect to the equilibrium PDF. If one wants to test the q exponential, the computation of excess kurtosis and skewness may not suffice since they become undefined for $q \gtrsim 1.2$. Thus we used the q exponential to fit the histograms of the r^2. We observed a strong dependence of the q exponential fit results on the amount of data in the histogram and in its binning [17]. For a solid result, we increased the decimated time buffer, respectively, by a factor 8 and 20 for the $m1$ and $m2$ oscillators (corresponding to a total time per histogram of 40 and 20 h respectively) before fitting the histograms, which we did for different bin widths. By comparing the results of the fits for the equilibrium data and for the maximum nonequilibrium, we found no change in the statistical distribution (apart for the slope of the exponential trend): the best values of q given by the fits change within the error. This reinforces the conclusions drawn above.

V. CONCLUSIONS

Given the observables we considered, looking only at the acquired signal and not knowing that a heat flux is circulating, the only way to distinguish that the oscillator is away from equilibrium is to compare the effective temperature resulting from the variance of the oscillator position with the average thermodynamic temperature: as discussed in Ref. [14], in both equilibrium and nonequilibrium steady states this is well mapped by the oscillator resonant frequency. Thus, provided one has calibrated the oscillator resonant frequency with a thermometer, one can solely use the oscillator position fluctuations to establish whether it is in equilibrium or not. Analogously to Ref. [18], the discrepancy between the thermodynamic temperature and the variance of the position (hence the effective temperature) allows one to ascertain the nonequilibrium nature of the state. There the nonequilibrium was caused by an electronic feedback that cooled the electromechanical oscillators of the gravitational wave detector AURIGA below the thermodynamic temperature. This is in agreement with the fact that nonequilibrium states do not necessarily imply non-Gaussian distributions for given observables.

The above results suggest a method to investigate nonequilibrium effects in gravitational wave interferometric detectors, which were our main motivation for starting this research [19]. To achieve the impressive sensitivity expected to allow a reasonable detection rate to the upcoming second generation [20], they consist of giant Michelson interferometers with optical resonant cavity arms, a few km in length, and suspended mirrors, about 40 kg in mass; circulating laser powers up to 760 kW are employed. Thermal noise of the mirrors and their suspensions is a major noise source. In spite of the high optical quality of the materials (mirror coatings and substrates), a fraction of the power is absorbed generating nonuniform

temperature fields in the optics: they cause mismatching of the interferometer resonant cavities and force the use of complex thermal compensation systems [21] to recover the ideal radius of curvature. As a result, the mirrors work in nonequilibrium states with thermal differences of the order of 20 K [22], around or just above room temperature: for the continuous operation of the detectors we can consider the states as being stationary. Hence from the thermodynamic viewpoint, the experimental situation does not differ substantially from ours: macroscopic elastic bodies with first resonances occurring in the same frequency range as ours, and subject to steady-state heat fluxes which cause temperature differences around room temperature similar to those of our experiment. Major differences come from the use of different materials (fused silica instead of the aluminium alloy of our experiment) and the fact that the out-of-resonance thermal noise is also of concern. Indeed, for what concerns the noise level near the mode resonances, our analysis of Sec. II indicates that the use of different materials (fused silica instead of the aluminium alloy of our experiment) does not lead to qualitatively different results: Fig. 2 shows that the specific interparticle potentials, which characterize the different materials, play no major role. Our results may thus apply to interferometers, and they suggest that the shape of the nonequilibrium distributions for the thermal noise of the mirrors must not sensibly depart from the equilibrium shape, and that the noise variance remains the only accessible quantity which can be used for a correct calibration of detectors, taking into account the dissipative phenomena. On the other hand, the effects of dissipation are crucial, differently from what previously believed, because they strongly alter the temperatures at which instruments are supposed to operate; hence they have a major impact on the quantitative analysis. In particular, they lead to noise levels corresponding to temperatures higher than those present in the instruments, an effect that could be interpreted otherwise as an error in the calibration. Our results indicate that a correct assessment of the nonequilibrium effects requires the measurement of the quantity a present in Eq. (6). For what concerns the out-of-resonance noise level, little can be anticipated and a dedicated study is mandatory.

ACKNOWLEDGMENTS

The research leading to these results has received funding from the European Research Council Starting Grant RareNoise (ERC-2007-StG – Grant No. 202680).

[1] M. Pitkin, S. Reid, S. Rowan, and J. Hough, Living Rev. Relativity **14**, 5 (2011).
[2] F. Ritort, in *Advances in Chemical Physics*, edited by S. A. Rice, Vol. 137 (John Wiley & Sons, Inc., Hoboken, NJ, USA, 2007).
[3] J. M. Ortiz de Zarate and J. V. Sengers, *Hydrodynamic Fluctuations in Fluids and Fluid Mixtures* (Elsevier, Oxford, 2006).
[4] G. M. Wang, E. M. Sevick, E. Mittag, D. J. Searles, and D. J. Evans, Phys. Rev. Lett. **89**, 050601 (2002).
[5] G. M. Wang, D. M. Carberry, J. C. Reid, E. M. Sevick, and D. J. Evans, J. Phys.: Condens. Matter **17**, S3239 (2005).
[6] G. M. Wang, J. C. Reid, D. M. Carberry, D. R. M. Williams, E. M. Sevick, and D. J. Evans, Phys. Rev. E **71**, 046142 (2005).
[7] M. E. J. Newman, Contemp. Phys. **46**, 323 (2005).
[8] U. M. B. Marconi, A. Puglisi, L. Rondoni, and A. Vulpiani, Phys. Rep. **461**, 111 (2008).
[9] T. Platini, Phys. Rev. E **83**, 011119 (2011).
[10] R. K. P. Zia and B. Schmittmann, J. Stat. Mech. (2007) P07012.
[11] L. Conti, P. De Gregorio, G. Karapetyan, C. Lazzaro, M. Pegoraro, M. Bonaldi, and L. Rondoni, J. Stat. Mech. (2013) P12003.
[12] A. Crisanti, A. Puglisi, and D. Villamaina, Phys. Rev. E **85**, 061127 (2012).
[13] P. De Gregorio, L. Rondoni, M. Bonaldi, and L. Conti, Phys. Rev. B **84**, 224103 (2011).
[14] L. Conti, P. De Gregorio, M. Bonaldi, A. Borrielli, M. Crivellari, G. Karapetyan, C. Poli, E. Serra, R. K. Thakur, and L. Rondoni, Phys. Rev. E **85**, 066605 (2012).
[15] A. Papoulis, *Probability, Random Variables, and Stochastic Processes*, 3rd ed (McGraw-Hill, New York, 1991).
[16] C. Tsallis, J. Stat. Phys. **52**, 479 (1988).
[17] E. Milotti, Phys. Rev. E **83**, 042103 (2011).
[18] M. Bonaldi *et al.*, Phys. Rev. Lett. **103**, 010601 (2009).
[19] L. Conti, M. Bonaldi, and L. Rondoni, Classical Quantum Gravity **27**, 084032 (2010).
[20] Advanced Virgo Baseline Design, The Virgo Collaboration, note VIR-027A-09 May 16, 2009, https://tds.ego-gw.it/itf/tds/file.php?callFile=VIR-0027A-09.pdf.
[21] J.-Y. Vinet, Living Rev. Relativity **12**, 5 (2009).
[22] R. C. Lawrence, Ph.D. thesis, Massachusetts Institute of Technology, 2003.